Fusion Bonding Possibility for Incompatible Polymers by the Novel Ultrasonic Welding Technology: Effect of Interfacial Compatibilization

Xie Fu,* Xueli Wu, Guigang Huang, Wenquan Li, Shuai Kang, Liang Wang, Jinling Luo, Ziwei Pan, and Wenqiang Lu*

ACCESS | Metrics & More | Article Recommendations

ABSTRACT: Fusion bonding for polymers has been successfully welded for the same and dissimilar materials. However, it is difficult to bond incompatible polymers due to poor interfacial adhesion. Usually, interfacial compatibilization can resolve this problem. According to the mechanism, an interlayer solder sheet (ISS) consisting of maleic anhydride-functionalized polypropylene (PP-g-MAH) and polyamide6 (PA6) was introduced into the ultrasonic welding (USW) device. In this way, it successfully realized the weldability between PP and PA6. The welding strength of PP−PA6 reached 22.3 MPa, about 84% welding strength for the PP body and 63% tensile strength for PP. Fourier transform infrared (FTIR) spectroscopy, X-ray diffraction (XRD), and scanning electron microscopy (SEM) showed the formation of PP-g-PA6 copolymer in blends. This copolymer played the role of an emulsifier, which enhanced the interfacial adhesion between PP and PA6 in two phases, leading to micron-scale homogeneity. In the USW process, the copolymer could act as a bridge between PP and PA6 molecular chains to realize the fusion bonding of incompatible polymers. Finally, we proposed the fusion bonding model for PP−PA6 interfaces.
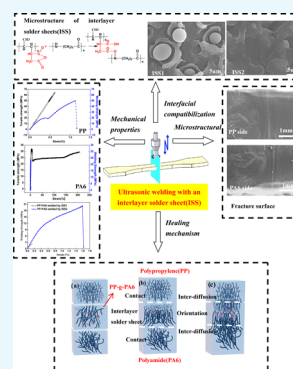
1. INTRODUCTION

Fusion or welding is widely used in the secondary assembly of plastics, showing great potential in medical equipment, automotive parts, aerospace materials, and other aspects. The efficiency of welded joints can be close to the bulk performance of thermoplastics.[1,2] Usually, fusion bonding can be divided according to the technology used for introducing heat, such as spin welding, vibration welding, microwave welding, ultrasonic welding (USW), and so on.[3−6] Through the above bonding techniques, many studies on welding of thermoplastics have been reported, including the same material and dissimilar materials, such as polyethylene (PE),[7] PP,[8] polyether ether ketone (PEEK),[9] acrylonitrile-butadiene-styrene (ABS) copolymer,[10] PA6,[11] PE-PP,[12] PA6-PA66,[13] polylactic acid-polyformaldehyde (PLA-POM),[14] PLA-poly(methyl methacrylate) (PMMA),[15,16] and PMMA-ABS.[17] Liu et al.[18] studied ultrasonic welding of a carbon fiber-reinforced nylon 66 composite without an energy director. To ensure joint strength, it was necessary to apply the proper weld schedules (i.e., welding time and horn pressure) in ultrasonic welding. Luciano et al.[19] summarized the weldability of thermoplastic materials for friction stir welding (FSW), which highlighted the joining of similar/dissimilar polymeric materials. However, they are compatible with each other. So far, there are few reports on fusion bonding for incompatible polymers.

For incompatible polymer blends, the formation of the molecular bridge becomes very difficult due to the obstacle to the interdiffusion of the molecular chains and the poor interfacial conditions.[20] The thin interfacial thickness and high interfacial tension can easily induce phase separation.[21] To resolve these problems, interfacial modification for incompatible polymers has been a major topic for researchers in the last decade. One way is to modify the incompatible polymeric blends by in situ chemical reactions to design model sequence-specific copolymers to minimize the energy of a polymer/polymer interface.[22−26] Another way of diminishing incompatibility is to add a copolymer, often a diblock copolymer, where the immiscible components are combined and form a relatively strong interface.[27−30] Wang et al.[31−33] adopted the strategy of organic surface modification by a chemical method to improve the interfacial adhesion of functional fillers to polymer matrix materials to strengthen the functionality of composites. Yu et al.[34] blended PLA with a soft and biodegradable polymer, poly[(butylene succinate)-co-adipate](PBSA), to improve the material mechanical properties and thermal properties based on in situ compatibilization. Therefore, to realize the weldability for
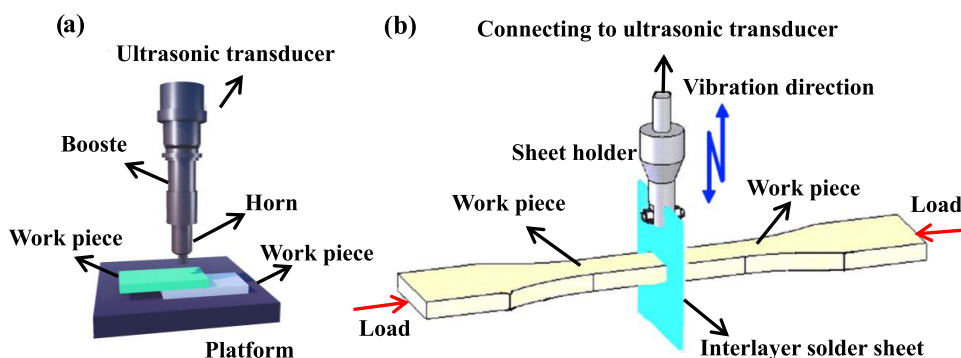
Figure 1. Welding principle for a traditional and a novel ultrasonic welding method: (a) traditional USW and (b) novel USW.
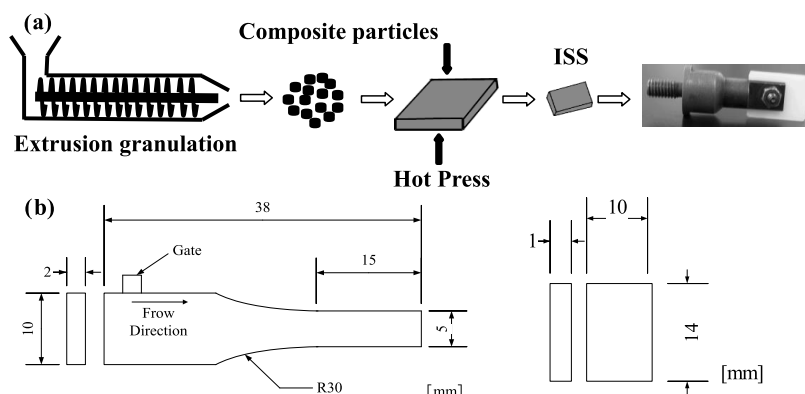

Figure 2. (a) Illustration of the ISS preparation method for welding between PP and PA6 and (b) dimensions of the workpiece (WP) geometry and ISS geometry.

incompatible materials, interfacial compatibilization may be a potential solution.

For the polypropylene (PP)/polyamide6 (PA6) system, the blend phase diagram shows a typical sea−island structure, which cannot realize fusion bonding for complete incompatibility.[35,36] Maleic anhydride-functionalized PP (PP-*g*-MAH) is usually used as a compatibilizer to modify the interfacial adhesion.[37] Many studies have concentrated on the fundamental understanding of the effect of this copolymer on the interfacial adhesion in the PP−PA6 reactive system.[38−41] In the PP-*g*-MAH/PA6 reactive system, the faster size reduction, finer particle size, better morphology stability, and a much thicker interface were obtained, ref 42. Restagno[43] studied the formation of diblock copolymers at the PP−PA6 interface to optimize the co-extruded PP−PA6 thin film. As expected, the grafting reaction of PP-*g*-MAH on the end groups of PA6 chains appeared fast and started even before PA6 was molten. Hu[44] showed that the emulsion-in-emulsion (EE) structure in the compatibilized PP−PA6 blends is an important factor leading to the continuous phase viscosity and the effective volume fraction of the dispersed phase. Based on previous research work, in the PP−PA6 reactive system, the PP-*g*-PA6 copolymer mainly played dual roles. One is the role of an emulsifier, which can reduce the interfacial tension and enhance the interface thickness. The other is to enhance the bonding force between the phases in the solid phase, thereby improving the mechanical properties.

Ultrasonic welding (USW) for both amorphous and semi-crystalline polymers is a very popular technique with many advantages such as fast, low cost, easy automation, and good joint.[45] The traditional USW method can realize the bonding for

polymers based on the stack of polymer sheets (Figure 1a). Its working principle is to convert alternating current into ultrasonic vibration, which reaches the interface through the workpiece and generates stress and strain in the contact area between the two workpieces, resulting in the heating and melting of the polymer. Then, the workpieces are pressed together under the load. Finally, after being resolidified, bonding is made.[46] The bonding process is governed by molecular chain diffusion and physical interaction to form chemical bonds. In this way, molecular bridges can be built between interfaces, and this process can be carried out well for most materials except for incompatible materials.

Based on traditional ultrasonic welding technology and interfacial modification for incompatible polymeric blends, an interlayer solder sheet (ISS) was fixed to the horn by the ISS holder and worked between the two workpieces. Through the interface compatibilization, the blends of PP-*g*-MAH/PA6 were made into ISS to realize weldability between the PP workpiece and the PA6 workpiece. Moreover, the relationship between the welding strength of PP−PA6 and the microstructure of ISS was studied. The possible healing of incompatible polymer−polymer interface was proposed.

2. BASIC WELDING PRINCIPLE

Figure 1b shows the schematic of the welding principle. The ISS is fixed by the ISS holder. Therefore, the ISS prepared by blending with different contents of PP-*g*-MAH or PP and PA6 can be connected to the holder. The two workpieces are symmetrically fixed on both sides of the ISS. Then, the ISS could join the two workpieces. During welding, the heat source mainly contains two parts. One is the intermolecular friction heat,

originating from the ultrasonic energy dissipated by viscoelastic polymers. The other is the frictional heat produced by the ultrasonic vibration at weld interfaces.[47,48]

3. EXPERIMENTAL SECTION

3.1. Materials. A commercial polypropylene (PP) with a melt index of 11 g/10 min was supplied by Polychem Co., Japan. The maleic anhydride-grafted PP (PP-*g*-MAH) with a maleic anhydride content of 0.8 wt % was supplied by Ketong Plastic CO., Ltd., Shenyang, China. Polyamide6 (PA6) was supplied by Toray Industries INC., Japan.

3.2. Preparation of Specimens. The workpieces with the shape of a half dumbbell were prepared using a common injection molding machine (FANUC Company, ROBOSHOT S2000i 100A), where half of the mold was taken up by a copper stick (Figure 2b). Before the injection molding process, the PP, PP-*g*-MAH, and PA6 were first dried in a vacuum oven at 80 °C for 24 h. Then, the PP and PA6 were injection-molded into the shape of a half dumbbell (Figure 2b). The injection molding conditions are listed in Table 1.

Table 1. Injection Molding Conditions for Welding Specimens

	PP	PA6
injection melt temperature (°C)	200	240
mold temperature (°C)	40	80
injection speed (mm/s)	53	53
injection pressure (MPa)	23	23
cooling time (s)	30	30

The ISS was prepared in three steps (Figure 2a). First, the mixtures of pure PP, PA6, blend of PA6 with 70% PP-*g*-MAH, and blend of PA6 with 70% PP were placed in a mixer for melt blending for 10 min at 240 °C. Second, the four types of materials were compressed into a rectangle with a thickness of 1 mm by a hot-press machine (IMOTD LTD.) (molding parameters: temperature of 240 °C and heating time of 10 min). Then, the ISS was cut as a rectangle with 14 × 10 × 1.0 mm³ dimensions (Figure 2b). Lastly, the middle part in the front edge of the ISS had broached a hole where the diameter was 3 mm for screw fixing.

3.3. Ultrasonic Welding. As shown in Figure 1b, the ISS was installed on the ISS holder with the screw fixed on the holder. Then, the workpieces were burnished with abrasive paper to enhance the interfacial friction. After burnishing, the workpieces were fixed on the two sides of the ISS under the load. Finally, the ultrasonic machine was turned on and the joints between ISS and workpieces were made. Welding conditions were as follows: a frequency of 28 kHz and an amplitude of 30 μm (constant). The welding time was usually varied from 1 to 8 s, while the welding stress was adjusted in the range of 01−1 Mpa. We set the welding stress as 0.6 MPa and welding time as 5 s after much exploration and optimization.

3.4. Testing and Microscopy. *3.4.1. DTA-TG Analysis.* The PP, PA6, and PP-*g*-MAH were measured using the DTA-TG apparatus (Shimadzu Corp., Model DTG-60) with a heart rate of 10 °C from 20 to 500 °C in air.

3.4.2. Tensile Test. After ultrasonic welding, the stress−strain behaviors of weld specimens were measured using a Universal tester (Series3360) operating in tension mode at 23 ± 2 °C. A crosshead speed of 10 mm/min was used in the test. The relative humidity was 50% (GB/T 1040.1−2018). The test spline was dumbbell type, and its size was L = 76 mm, W = 10 mm, and d = 1 mm.

3.4.3. SEM Analysis. The tensile fracture surfaces of the specimens were examined using a scanning electron microscope (SEM, S-4300, Hitachi) to analyze the relation between welding strength and interfacial morphology. To study the phase dispersion, the quenched specimen was fractured in liquid nitrogen, and the fracture surface was observed using SEM.

3.4.4. Dispersed Phase in ISS Extraction. The blends of PP-*g*-MAH/PA6 and PP−PA6 with a mass ratio of 70:30 were dissolved in formic acid at room temperature for 120 h to remove unreacted PA6. Then, the samples were washed with fresh solvent and dried at 50 °C until a constant weight was attained.

3.4.5. FTIR Analysis. The diluted components were prepared for Fourier transform infrared (FTIR) measurement. The FTIR spectra were recorded on a Jasco MFT-2000 spectrophotometer between 4000 and 600 cm⁻¹, at a resolution of 4 cm⁻¹, using sample films.

3.4.6. XRD Analysis. Wide-angle X-ray spectra were recorded with a D 500 diffractometer (Siemens) in step scan mode using Ni-filtered Cu Kα radiation (0.1542 nm wavelength). Powder samples were scanned in reflection, whereas the injection-molded compounds were scanned in transmission in the interval of 2θ = 2−10°. The interlayer spacing of the organoclay was derived from the peak position (d_{001}-reflection) in the X-ray
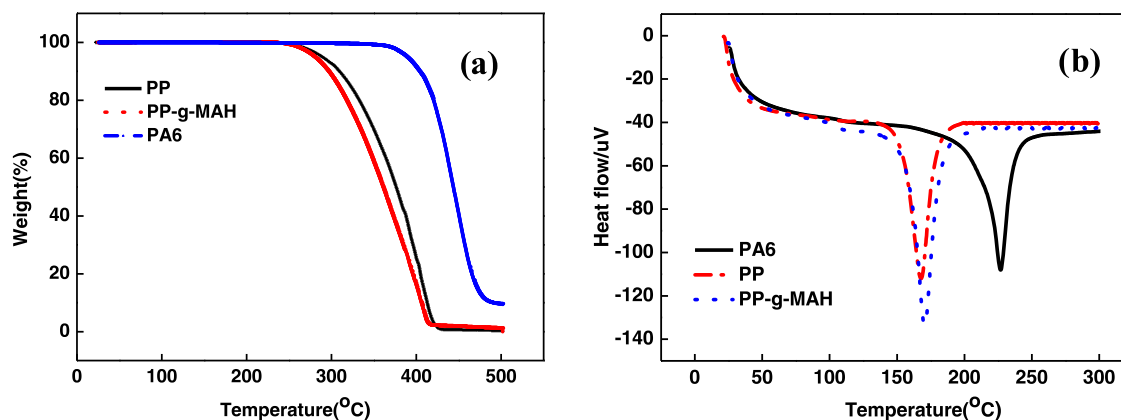

Figure 3. (a) TG test of PP, PP-*g*-MAH, and PA6 and (b) TDA test of PP, PP-*g*-MAH, and PA6.
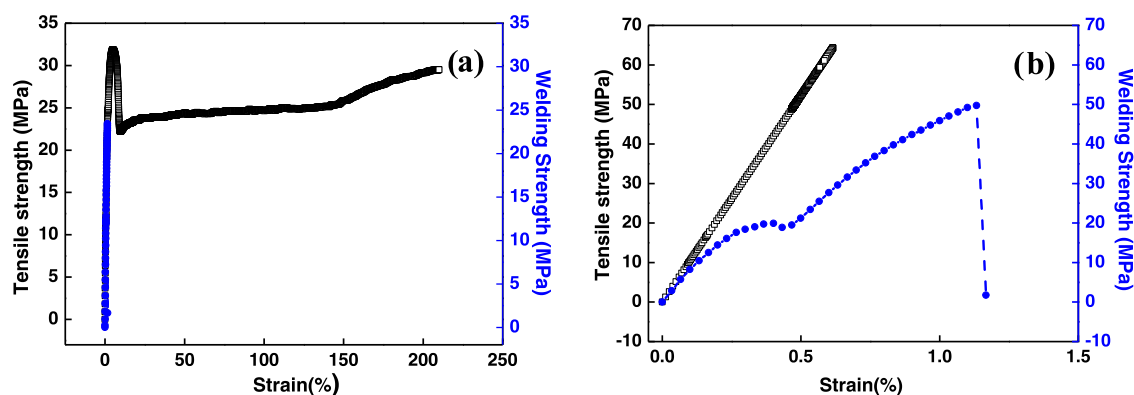
Figure 4. Tensile and welding strength curves of (a) PP and (b) PA6.

diffraction (XRD) diffractograms according to the Bragg equation.

4. RESULTS AND DISCUSSION

4.1. Thermal Performance Analysis. Figure 3a shows the weight loss vs temperature curves of pure polypropylene (PP), polyamide6 (PA6), and polypropylene-grafted maleic anhydride(PP-*g*-MAH), which are heated up to 500 °C in air. The inset shows the weight loss between 250 and 420 °C for PP and PP-*g*-MAH with a minor difference. However, the weight loss of PA6 started from 360 to 490 °C. The distinction of degradation temperature windows between PP, PP-*g*-MAH, and PA6 inevitably affects the fusion bonding between the two materials. From Figure 3b, the DTA cures of three materials also showed some degree of difference in melting points between PP, PP-*g*-MAH, and PA6. T_m of PP and PP-*g*-MAH was close to 170 °C, while T_m of PA6 was about 225 °C, which ensured a reasonable processing window for PP and PA6. Compared with PP, the molecular chain of PA6 contained large polar groups, resulting in a rigid molecular chain and strong intermolecular force. In addition, the molecular weight of PA6 was higher than that of PP. Therefore, there was a certain difference in the melting temperature of PA6 and PP from the DTA curve.

4.2. Mechanical Properties and Welding Properties of Pure PP and PA6. As a result of the test carried out on the Universal tester (Series3360), Figure 4 shows the curves of the tensile strength and welding strength with strain for PP and PA6. From Figure 4a, the mechanical performance for PP showed the typical characteristics of ductile materials. The tensile strength of PP attained was 32 MPa with 210% strain. Moreover, the welding strength of PP approached 24 MPa, about 75% tensile strength of PP. Meanwhile, the stress−strain curve of polyamide6 showed the typical brittle material characteristics (Figure 4b). The tensile strength of PA6 was about 64 MPa. The welding strength of PA6 was close to 50 MPa, about 78% of the tensile strength of PA6.

4.3. Weldability between PP and PA6. From previous statements, to realize the fusion boding possibility for PP and PA6, we introduced the ISS. According to the interfacial compatibilization mechanism, the PP-*g*-MAH and PP were blended with PA6 with a mass ratio of 70:30 to prepare the ISS1(PP−PA6) and ISS2(PP-*g*-MAH/PA6).

Under the same welding process parameters (welding load, 6N and welding time 5S), the ISS1 and ISS2 were introduced for the welding of PP and PA6. Then, after the tensile test, the welding curve for PP−PA6 is obtained, as shown in Figure 5. The welding strength of PP−PA6 by ISS1 was only 2.4 MPa,
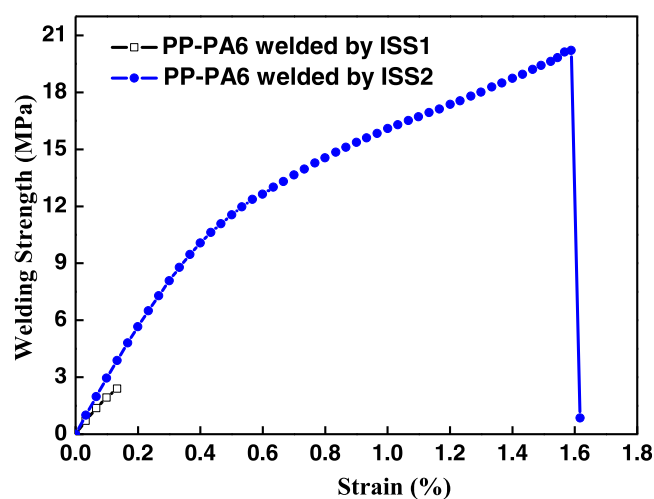

Figure 5. Welding strength of PP−PA6 by ISS1 and ISS2 (ISS1: blends of PP and PA6 at 70:30; ISS2: blends of PP-*g*-MAH and PA6 at 70:30).

which almost indicated welding failure between PP and PA6. But the welding strength of PP−PA6 by ISS2 reached 22.2 MPa, almost 10 times higher than the welding strength of PP−PA6 by ISS1. Moreover, this value was about 84% welding strength for the PP body, 63% tensile strength for PP, which showed that the ISS2 by interfacial compatibilization successfully achieved fusion bonding between PP and PA6 under ultrasonic welding.

Furthermore, we analyzed the fracture morphologies using SEM. From Figure 6a,b, the fracture surface on both the PP and PA6 sides showed rough, irregular morphologies. Amazingly, there were some areas unwelded on the PA6 side, which is demonstrated in Figure 6c. Compared with the fracture surface for PP/ISS1/PA6, Figure 6d,e shows perfect welding fracture surfaces.

Whether the PP side or the PA6 side, the morphologies were smooth and uniform, which showed typical homogeneity at a five-micron scale (Figure 6f). Therefore, the weldability of PP and PA6 may depend on the properties of ISS, such as components in ISS, affinity with workpieces on both sides, and interfacial adhesion of molecular chains.

4.4. Tensile Properties and Morphologies of ISS1 and ISS2. The large discrepancy in welding strength for these two welding specimens might be due to the plasticity and dissimilar molecular chain interfacial tension and thickness of PP−PA6 and PP-*g*-MAH/PA6 blends.

To illustrate this phenomenon, Figure 7 shows the tensile properties and morphologies of ISS1 and ISS2. The tensile
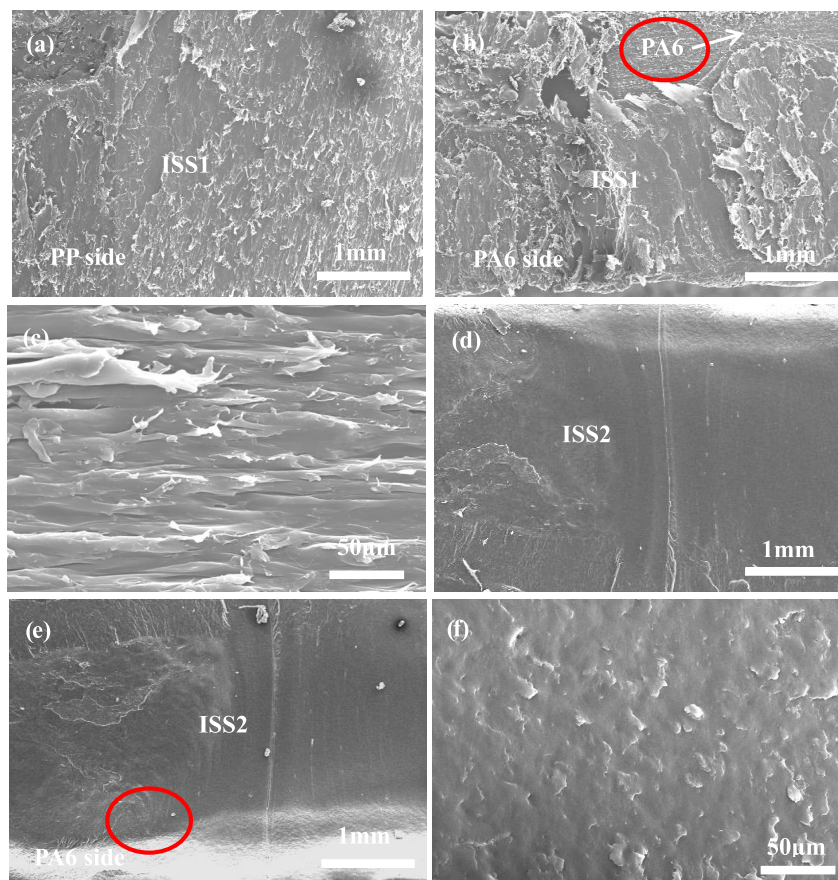
Figure 6. Scanning electron micrographs of the welding fracture surface for PP/ISS/PA6 welding joints. (a) PP side on the ISS1, (b) and (c) PA6 side on the ISS1, (d) PP side on the ISS2, and (e) and (f) PA6 side on the ISS2.
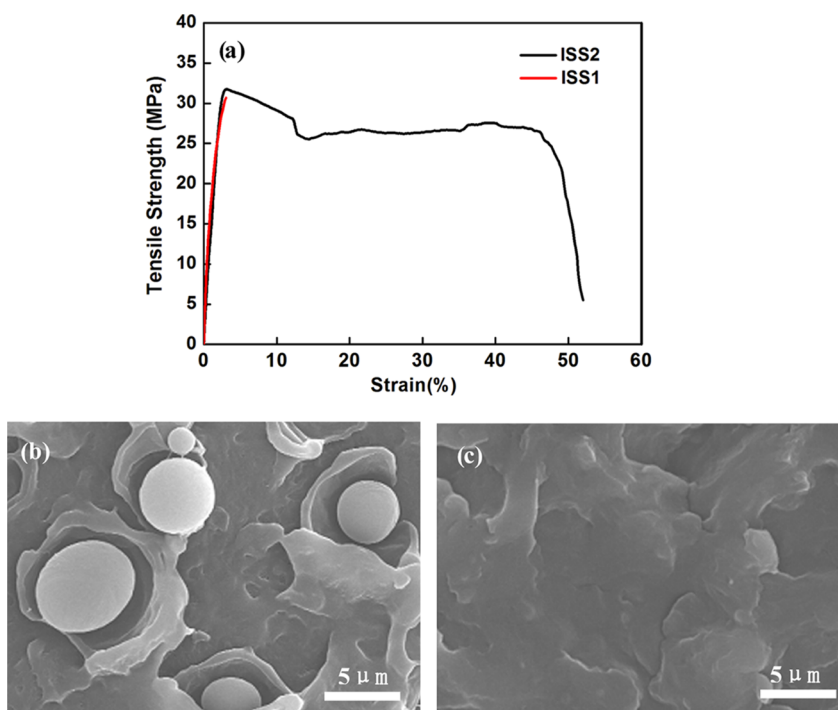

Figure 7. Tensile properties and morphologies of interlayer solder sheet (ISS): (a) tensile properties of ISS1 and ISS2; (b) morphologies of ISS1: blend of PP and PA6; and (c) morphologies of ISS2: blend of PP-*g*-MAH and PA6.
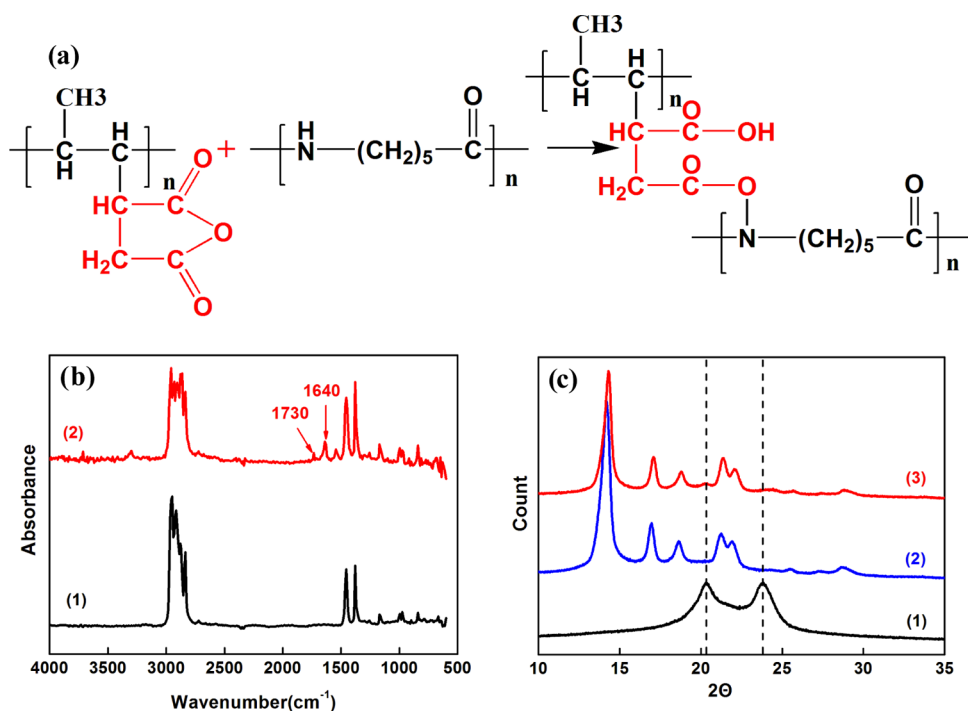
Figure 8. (a) Chemical reaction principle and (b) infrared spectra analysis for the ISS: (1) ISS1 with the extraction of PA6 and (2) ISS2 with the extraction of PA6. (c) XRD analysis for the ISS: (1) pure PA6, (2) ISS1 with the extraction of PA6, and (3) ISS2 with the extraction of PA6.

strength of the two blends was higher than 30 MPa. The toughness of PP-*g*-MAH/PA6 blends was significantly improved (Figure 7a), which could provide plasticity to dissipate ultrasonic energy, and conducive to the conversion of ultrasonic energy into molecular chain energy during welding.

The dispersed particles debonded with the matrix, and individual PA6 particles appeared. ISS1 showed a typical sea—island structure (PP—PA6 blends with 70:30), suggesting weak interfacial adhesion (Figure 7b).

In contrast, it was difficult to distinguish individual particles in the 70:30 PP-MAH/PA6 (ISS2) blend system. There was almost no phase separation between PP-*g*-MAH and PA6. This might suggest stronger adhesion between PP-*g*-MAH and PA6 due to the formation of block copolymers at the interface (Figure 7c). The strong interfacial adhesion was sufficient for plastic deformation, which resulted in substantially improving energy dissipation. Therefore, the ISS2 could dissipate energy into the friction heat of molecular chains much easier than ISS1 during the ultrasonic welding between PP and PA6. Thus, the interfacial diffusion and molecular bridge between the two weld interfaces could be established. This might be the potential reason for the specimen welded by ISS2 obtaining a higher welding strength compared with the specimen welded by ISS1.

4.5. Characterization of the PP-g-PA6 Copolymer. In general, a reactive compatibilizer can produce a graft or block copolymer that contains segments miscible or compatible with both components in the blend. For the PP-*g*-MAH/PA6 blend, the succinic anhydride groups on PP-*g*-MAH were able to react with the PA6 amine terminal groups to form a PP-*g*-PA6 copolymer during melt processing. Figure 8a predicts the chemical reaction principle between PP-*g*-MAH and PP. To clarify this predicted reaction, the PA6 domains were removed by formic acid. Figure 8b shows the FTIR spectra of (1) ISS1 with the extraction of PA6 and (2) ISS2 extraction with PA6. From the spectra b1, only the information of the PP molecules

was obtained, which indicated no chemical bonding reaction between PP and PA6. However, spectra b2 exhibited absorbances at 1640 and 1730 cm^{-1}, which were attributed to vibrations of the PA6 carbonyl group and carbonyl amide linkage, respectively. This indicated that the PP-*g*-PA6 copolymer was formed at the interface.

Moreover, Figure 8c shows the XRD spectra of (1) pure PA6, (2) ISS1 with the extraction of PA6, and (3) ISS2 with the extraction of PA6. Figure 8c3 shows a still small PA6 diffraction peal, whereas no information on PA6 was obtained (Figure 8c2). This might result from the fractionated crystallization of PA6 in the PP-*g*-PA6 copolymer. As the PP-g-PA6 copolymer was believed to act as the emulsifier to attain the size reduction to a sub-micrometer level, it provided a finer dispersion morphology and increased the adhesive strength between the two phases. Therefore, during the ultrasonic welding, these copolymers in the ISS2 could increase the mobility of the molecules to the interface (plastic effect) and promote the fusion bonding formation at both PP and PA6 sides.

4.6. Fusion Bonding for PP—PA6 under Different ISS Components. PP-*g*-PA6 could promote wetting at the interface and increase molecular mobility. Therefore, we needed to analyze the welding performance of PP—PA6 under different ISS components (Figure 9). From the curve of welding strength with different PP-*g*-MAH contents, the better values with PP-*g*-MAH contents varied from 30 to 70%. When the contents of one phase in ISS2 were too low (PP-*g*-MAH content: 10% or PA6 content: 10%), the welding strength dramatically decreased, which might be relative to the healing process during ultrasonic welding. Before welding, the surface morphologies of PP and PA6 specimens were relatively flat, with a certain roughness (Figure 10a,b). When PP-*g*-MAH or PA6 contents were too low, the fracture surfaces were uneven and rough and even showed unbonded parts. This was due to a lack of PP-*g*-PA6, the poor interface of PP/ISS2 or PA6/ISS2 wetting, and the interdiffu-
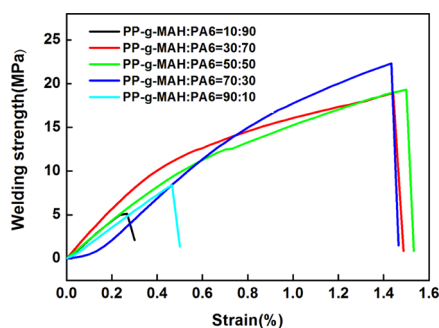
Figure 9. Welding performance of ISS with different PP-*g*-MAH contents on PP-PA.

sion obstacle of the molecular chain, resulting in a nonideal state of the healing process. However, when the PP-*g*-MAH content was 50%, the fracture surfaces were smoother and showed better integrity (Figure 10e,f). The ISS2 fully bonded with the PP side or the PA6 side. Excellent welding strength and perfect welding cross section proved that PP/ISS2 and PA6/ISS2 interfaces were well cured.

4.7. Fusion Bonding Model for PP−PA6 Interfaces. Wool first proposed the healing mechanism of a polymer−polymer interface.[49] There were five sequential stages:[50] (1) surface−rear arrangement, (2) surface approach, (3) wetting, (4) diffusion, and (5) solidification. For similar polymer bonding, molecular chains were easier to wet and diffuse. Therefore, the two distinct interfaces could be diffused across

each other, followed by autohesion and consolidation. However, when bonding an incompatible polymer interface, it became difficult. To resolve these problems, the compatibilizers play a key role. Simmon[51] indicated that designing sequence-specific copolymer compatibilizers, which have been employed to enhance material properties in settings ranging from emulsions to polymer blends, could improve the stability of an interface.

According to FTIR and DSC curves, the PP-*g*-PA6 copolymer was formed in the blends of ISS2. The two distinct interfaces of PP/ISS2 and ISS2/PA6 still existed before ultrasonic welding (Figure 11a). At the initial stage of ultrasonic application, PP-*g*-PA6 played the role of an emulsifier composed of distinct repeat units with preferential orientation and affinity for each of the two incompatible phases (PP and PA6) (Figure 11b). With the conversion of ultrasonic energy into frictional heat, the polar PA6 and nonpolar PP molecular chain migrate to the PP and PA6 welding interface, respectively, and produce wetting and interdiffusion under the promotion of ultrasonic energy. Meanwhile, the PP-*g*-PA6 copolymer as a bridge connected each other (Figure 11c). In this way, the potential barriers associated with inhomogeneities at the interface disappeared. The two molecular chains were free to move across the two interfaces. Then, after solidification, the two incompatible workpieces could be fusion-bonded. Thus, a molecular chain bridge was formed, and quick autoadhesion of the two interfaces for PP/ISS2 and PA6/ISS2 could be performed.
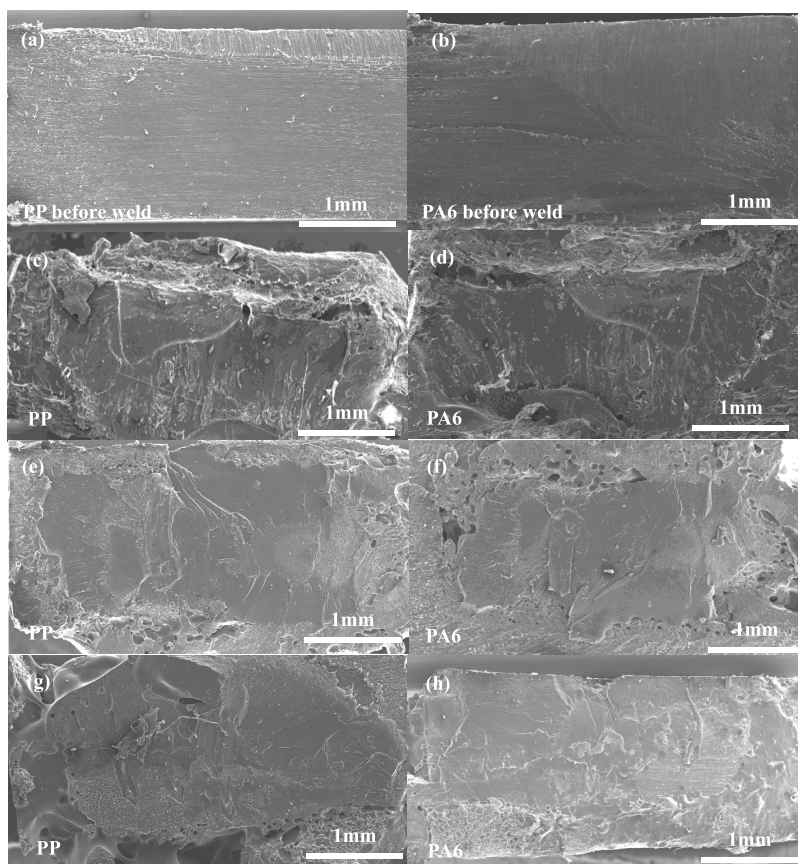

Figure 10. Morphologies of welding section with different ISS2 compositions. (a) PP before weld; (b) PA6 before weld; (c) PP side, ISS2 with 10% PP-*g*-MAH; (d) PA6 side, ISS2 with 10% PP-*g*-MAH; (e) PP side, ISS2 with 50% PP-*g*-MAH; (f) PA6 side, ISS2 with 50% PP-*g*-MAH; (g) PP side, ISS2 with 90% PP-*g*-MAH; and (h) PA6 side, ISS2 with 90% PP-*g*-MAH.
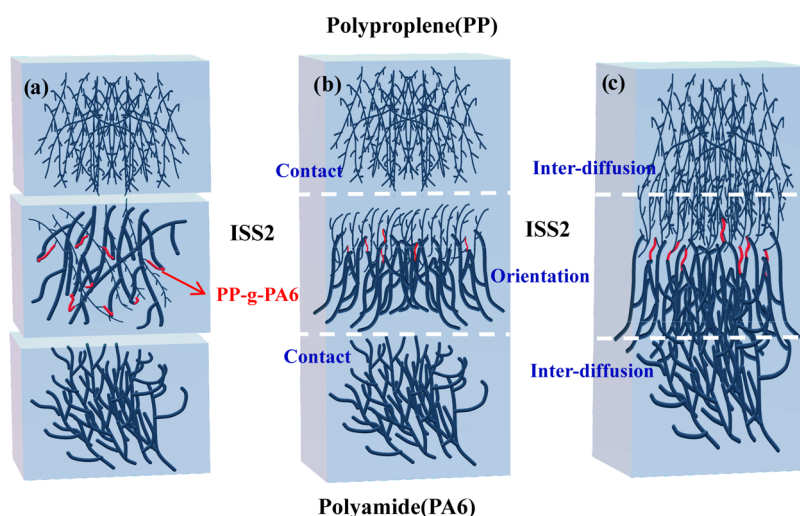
Figure 11. Healing of PP−PA6 interfaces showing (a) two distinct interfaces, (b) achievement of intimate contact, and (c) collapse of the interface through interdiffusion.

5. CONCLUSIONS

Our study on the fusion bonding possibility for incompatible polymers by USW showed the following.

(1) The incompatible polymers polypropylene (PP) and polyamide6 (PA6) could be successfully welded by the ultrasonic welding method, through the introduction of an ISS and interfacial modification.

(2) The welding strength of PP−PA6 by ISS2 reached 22.3 MPa, about 84% welding strength for the PP body and 63% tensile strength for PP.

(3) The PP-*g*-PA6 copolymer played the role of an emulsifier to enhance the interfacial adhesion between PP and PA6 in two phases, leading to a micron-scale homogenous structure in ISS2.

(4) The fusion bonding model for PP−PA6 interfaces was proposed. The copolymer PP-*g*-PA6 acted as a bridge between PP and PA6 molecular chains in ISS2. Under ultrasonic welding, the PP and PA6 molecular chains were free to move across the two interfaces (PP/ISS2 and PA6/ISS2), promoting the formation of a better welding interface after solidification.

■ AUTHOR INFORMATION

Corresponding Authors

Xie Fu − *Key Laboratory of Multi-Scale Manufacturing Technology, Chongqing Institute of Green and Intelligent Technology, Chinese Academy of Sciences, Chongqing 400714, P. R. China; College of Mechanical Engineering, Chongqing University, Chongqing 400714, P. R. China;* ⊙ orcid.org/0000-0002-2671-5464; Email: fuxie@cigit.ac.cn

Wenqiang Lu − *Key Laboratory of Multi-Scale Manufacturing Technology, Chongqing Institute of Green and Intelligent Technology, Chinese Academy of Sciences, Chongqing 400714, P. R. China;* Email: wqlu@cigit.ac.cn

Authors

Xueli Wu − *Department of Advanced Materials Science, Graduate School of Frontier Science, The University of Tokyo, Kashiwa 277-8561 Chiba, Japan*

Guigang Huang − *Chongqing Chenrui New energy technology Co., LTD., Chongqing 409099, P. R. China*

Wenquan Li − *Chongqing Jinshan Yangsheng Pipeline Co., Ltd., Chongqing 400014, P. R. China*

Shuai Kang − *Key Laboratory of Multi-Scale Manufacturing Technology, Chongqing Institute of Green and Intelligent Technology, Chinese Academy of Sciences, Chongqing 400714, P. R. China;* ⊙ orcid.org/0000-0002-8174-8605

Liang Wang − *Key Laboratory of Multi-Scale Manufacturing Technology, Chongqing Institute of Green and Intelligent Technology, Chinese Academy of Sciences, Chongqing 400714, P. R. China;* ⊙ orcid.org/0000-0002-6712-6500

Jinling Luo − *Key Laboratory of Multi-Scale Manufacturing Technology, Chongqing Institute of Green and Intelligent Technology, Chinese Academy of Sciences, Chongqing 400714, P. R. China*

Ziwei Pan − *Key Laboratory of Multi-Scale Manufacturing Technology, Chongqing Institute of Green and Intelligent Technology, Chinese Academy of Sciences, Chongqing 400714, P. R. China*

Complete contact information is available at:
https://pubs.acs.org/10.1021/acsomega.2c00255

Notes

The authors declare no competing financial interest.

■ ABBREVIATION

PP	polypropylene
PA6	polyamide6
ISS	interlayer solder sheet
PP-*g*-MAH	maleic anhydride-functionalized polypropylene
USW	ultrasonic welding
FSW	friction stir welding
WPs	workpiece
PE	polyethylene
PEEK	polyether ether ketone
ABS	acrylonitrile-butadiene-styrene copolymer

PA66   polyamide66
PLA   polylactic acid
POM   polyformaldehyde
PMMA   poly(methyl methacrylate)
EE   emulsion-in-emulsion

■ REFERENCES

(1) Oliveira, J. P.; Santos, T. G.; Miranda, R. M. Revisiting fundamental welding concepts to improve additive manufacturing: From theory to practice. *Prog. Mater. Sci.* **2020**, *107*, No. 100590.

(2) Palardy, G.; Shi, H.; Levy, A.; LeCorre, S.; Villegas, I. F. A study on amplitude transmission in ultrasonic welding of thermoplastic composites. *Composites, Part A* **2018**, *113*, 339−349.

(3) Barmouz, M.; Shahi, P.; Asadi, P. Friction stir welding/processing of polymeric materials. *Adv. Frict. Stir Weld. Process.* **2014**, *35*, 601−670.

(4) Poyraz, S.; Zhang, L.; Schroder, A.; Zhang, X. Ultrafast Microwave Welding/Reinforcing Approach at the Interface of Thermoplastic Materials. *ACS Appl. Mater. Interfaces* **2015**, *7*, 22469−22477.

(5) Chen, Y. J.; Yue, T. M.; Guo, Z. N. Combined effects of temperature field and ultrasonic vibration on bubble motion in laser joining of plastic to metal. *J. Mater. Process. Technol.* **2021**, *288*, No. 116846.

(6) Sadeghian, N.; Givi, M. K. B. Experimental optimization of the mechanical properties of friction stir welded Acrylonitrile Butadiene Styrene sheets. *Mater. Des.* **2015**, *67*, 145−153.

(7) Arici, A.; Sinmazelk, T. Effects of double passes of the tool on friction stir welding of polyethylene. *J. Mater. Sci.* **2005**, *40*, 3313−3316.

(8) Li, W.; Frederick, H.; Genevieve, P. Multifunctional films for thermoplastic composite joints: Ultrasonic welding and damage detection under tension loading. *Composites, Part A* **2021**, *141*, No. 106221.

(9) Tsiangou, E.; Kupski, J.; de Freitas, S. T.; Benedictus, R.; Villegas, I. F. On the sensitivity of ultrasonic welding of epoxy- to polyetheretherketone (PEEK)-based composites to the heating time during the welding process. *Composites, Part A* **2021**, *114*, No. 106334.

(10) Sadeghian, N.; Givi, M. K. B. Experimental optimization of the mechanical properties of friction stir welded Acrylonitrile Butadiene Styrene sheets. *Mater. Des.* **2015**, *67*, 145−153.

(11) Panneerselvam, K.; Lenin, K. Joining of Nylon 6 plate by friction stir welding process using threaded pin profile. *Mater. Des.* **2014**, *53*, 302−307.

(12) Rezaee Hajideh, M.; Farahani, M.; Alavi, SAD.; Ramezani, N. M. Investigation on the effects of tool geometry on the microstructure and the mechanical properties of dissimilar friction stir welded polyethylene and polypropylene sheets. *J. Manuf. Mater. Process.* **2017**, *26*, 269−279.

(13) Bates, P. J.; Dyck, C.; Osti, M. Vibration welding of Nylon 6 to Nylon 66. *Polym. Eng. Sci.* **2004**, *44*, 760−771.

(14) Zhang, G. H.; Qiu, J. H.; Sakai, E.; Zhou, Z. W. Interface investigation between dissimilar materials by ultrasonic thermal welding by the third phase. *Int. J. Adhes. Adhes.* **2021**, *104*, No. 102722.

(15) Zhang, G. H.; Qiu, J. H.; Shao, L.; Fu, X. Molecular Interdiffusion of Hauling Theory between Dissimilar Polymers Based on Novel USW. *Adv. Mater. Res.* **2011**, *221*, 289−294.

(16) Zhang, G. H.; Qiu, J. H.; Shao, L.; Liu, M. Z.; Zhang, M.; Wu, Yb. Ultrasonic weld properties of heterogeneous polymers Polylactide and poly(methyl methacrylate). *J. Mater. Process. Technol.* **2011**, *211*, 1358−1363.

(17) Dashatan, S. H.; Azdast, T.; Ahmadi, S. R.; Bagheri, A. Friction stir spot welding of dissimilar polymethyl methacrylate and acrylonitrile butadiene styrene sheets. *Mater. Des.* **2013**, *45*, 135−141.

(18) Yang, L.; Jorge, A.; Liu, Z.; Tae, H. L.; Fan, H. T.; Xiao, G.; Mihaela, B.; Jack, H. S. Ultrasonic Welding of Carbon Fiber Reinforced Composite With Variable Blank Holding Force. *J. Manuf. Sci. Eng.* **2018**, *140*, No. 091011.

(19) Kumar, R.; Kumar, R.; Singh, P. S. I.; Ahuja, R.; Penna, L. Weldability of thermoplastic materials for friction stir welding- A state of art review and future applications. *Composites, Part B* **2018**, *137*, 1−15.

(20) Alkhodairi, H.; Russell, S. T.; Pribyl, J.; Benicewicz, B. C.; Kumar, S. K. Compatibilizing Immiscible Polymer Blends with Sparsely Grafted Nanoparticles. *Macromolecules* **2020**, *53*, 10330−10338.

(21) Kim, D.; Sihn, M. R.; Jeon, M. G.; Yuan, G. C.; Satijia, S. K.; Kim, Y.; Choi, J. Non-equilibrium phase behavior of immiscible polymer-Grafted Nanoparticles Blends. *Macromolecules* **2019**, *52*, 5811−5818.

(22) Qin, L. J.; Qiu, J. H.; Liu, M. Z.; Fu, Xie.; et al. Mechanical and thermal properties of poly(lactic acid) composites with rice straw fiber modified by poly(butyl acrylate). *Chem. Eng. J.* **2011**, *166*, 772−778.

(23) Satyanarayana, M.; Sreenath, P. R.; Bhowmick, A. K.; Kumar, K. D. Catalyst driven preferential growth of in-situ generated nanosilica particles in the phases of incompatible polymer blend and its effect on physico-mechanical properties. *Polymer* **2018**, *156*, 186−202.

(24) Lv, J. W.; Zheng, C.; Hang, W.; Qin, T. J.; Liu, J. Q.; Liu, X. Y. In-situ polymerization and covalent modification on aramid fiber surface via direct fluorination for interfacial enhancement. *Composite, Part B* **2020**, *182*, No. 107608.

(25) Gao, C.; Zhang, S.; Li, X.; Zhu, S.; Jiang, Z. Synthesis of poly(ether ether ketone)-block-polyimide copolymer and its compatibilization for poly(ether ether ketone)/thermoplastic polyimide blends. *Polymer* **2014**, *55*, 119−125.

(26) Han, Di.; Wen, T.-j.; Han, G.; Deng, Y.-y.; Deng, Y.; Zhang, Q.; Fu, Q. Synthesis of Janus POSS star polymer and exploring its compatibilization behavior for PLLA/PCL polymer blends. *Polymer* **2018**, *136*, 84−91.

(27) Pu, S.; Hao, Y.-B.; Dai, X.-X.; Zhang, P.-P.; Zeng, J.-B.; Wang, M. Morphological, rheological, crystalline and mechanical properties of ethylene-vinyl acetate copolymer/linear low-density polyethylene/amphiphilic graphene oxide Nanocomposites. *Polym. Test.* **2017**, *63*, 289−297.

(28) Tan, Y.-J.; Li, J.; Chen, Y.-F.; Tang, X.-H.; Cai, J.-H.; Liu, J.-H.; Wang, M. Gentle crosslinking to enhance interfacial interaction in thermoplastic polyurethane/ poly(ethylene-co-1-octene)/multi-walled carbon nanotube composites for conductive improvement and piezoresistive stability. *Poly. Test.* **2019**, *75*, 142−150.

(29) Zhang, K.; Yu, H.-O.; Shi, Y.-D.; Chen, Y.-F.; Zeng, J.-B.; Guo, J.; Wang, B.; Guo, Z.; Wang, M. Morphological regulation improved electrical conductivity and electromagnetic interference shielding in poly(l-lactide)/poly(ε-caprolactone) / carbon nanotube nanocomposites viaconstrusting stereocomplex crystallites. *J. Mater. Chem. C* **2017**, *5*, 2807−2817.

(30) Ojijo, V.; Ray, S. S. Super toughened biodegradable polylactide blends with non-linear copolymer interfacial architecture obtained via facile in-situ reactive compatibilization. *Polymer* **2015**, *80*, 1−17.

(31) Cho, D. M.; Hu, W. C.; Koberstein, J. T.; Lingelser, J. P.; Gallot, Y. Segregation dynamics of block copolymers to immiscible polymer blend interfaces. *Macromolecules* **2000**, *33*, 5245−5251.

(32) Wang, Y.; Zhang, S.; Jiang, H.; Lin, Y.; Xing, H.; Tang, T. Insight on compatibilization of LLDPE/PS blends from morphology, interfacial state, mechanical properties and melt properties: Comb-like copolymer vs diblock copolymer. *Polymer* **2021**, *218*, No. 123540.

(33) Fu, Z.; Wang, H.; Zhao, X.; Horiuchi, S.; Li, Y. Immiscible polymer blends compatibilized with reactive hybrid nanoparticles: Morphologies and properties. *Polymer* **2017**, *132*, 353−361.

(34) Yu, Y. D.; Mu, Z.; Jin, B.; Liu, Z. M.; Tang, R. K. Organic-inorganic copolymerization for homogenous composite without interphase boundary. *Angew. Chem., Int. Ed.* **2020**, *59*, 2071−2075.

(35) Shokoohi, S.; Arefazar, A.; Nader, G. Compatibilized Polypropylene/Ethylene−Propylene−Diene-Monomer/Polyamide6 ternary blends: Effect of twin-screw extruder processing parameters. *Mater. Des.* **2011**, *32*, 1697−1703.

(36) Barangi, L.; Taromi, F. A.; Nazockdast, H.; Sararoudi, S. S. et al. *Interfacial Elasticity of Reactively Compatibilized PP/PA6 Blends. International Congress on Rheology*, The Society of Rheology 80th Annual Meet, American Institute of Physics, 2008, pp 1075−1079.

(37) Gil, B. M.; Song, S. W.; Lee, J. H.; Jeon, J.; Lee, K. H.; Wie, J. J. Introduction of primary chemical bonding in lignin-based PP composites for mechanical reinforcement via reactive extrusion. *Composite, Part B* **2019**, *165*, 510−515.

(38) Tokumitsu, K.; Nakajima, Y.; Aoki, K. Mechanical Properties of PP/PA Blends in Addition with PP-g-MAH with Different PP Molecular Weight and MAH Content. *AIP Conf. Proc.* **2016**, *1713*, No. 050006.

(39) Liu, H.; Xie, T.; Ying, Z.; Ou, Y.; Yang, G. Phase Morphology Development in PP/PA6 Blends Induced by a Maleated Thermoplastic Elastomer. *J. Polym. Sci., Part B: Polym. Phys.* **2006**, *44*, 1050−1061.

(40) Wang, D. X.; Xu, M. Novel strategy for ternary polymer blend compatibilization. *Polymer* **2006**, *47*, 7859−7863.

(41) Wang, Q.; Liu, C. S.; Chen, Z. Pan-milling preparation of polypropylene-graft-maleic anhydride and its compatibilizing effect on polyamide 6/polypropylene blend. *Polym. J.* **2001**, *33*, 522−527.

(42) Afsari, B.; Mir Karim, R. A.; Hasanpour, M. Evolution of morphology and morphology stability in PP/PA6/EPDM-g-MA reactive ternary blends using viscoelastic measurement. *Rheol. Acta* **2020**, *59*, 399−414.

(43) Barraud, T.; Restagno, F.; Devisme, S.; Creton, C.; Léger, L. Formation of diblock copolymers at PP/PA6 interfaces and their role in local crystalline organization under fast heating and cooling conditions. *Polymer* **2012**, *53*, 5138−5145.

(44) Shi, D.; Hu, G. H.; Ke, Z.; Li, R.K.Y.; Yin, J. H. Relaxation behavior of polymer blends with complex morphologies: Palierne emulsion model for uncompatibilized and compatibilized PP/PA6 blends. *Polymer* **2006**, *47*, 4659−4666.

(45) Tsiangou, E.; de Freitas, S. T.; Villegas, I. F.; Benedictus, Rinze. Investigation on energy director-less ultrasonic welding of polyetherimide (PEI)- to epoxy-based composites. *Composites, Part B* **2019**, *173*, No. 107014.

(46) Zhao, T.; Zhao, Q.; Wu, W.; Xia, L.; Lia, Y.; Wan, Z.; Villegas, I. F.; Benedictusc, R. Enhancing weld attributes in ultrasonic spot welding of carbon fiber-reinforced thermoplastic composites: Effect of sonotrode configurations and process control. *Composites, Part B* **2021**, *211*, No. 108648.

(47) Koutras, N.; Amirdine, J.; Boyard, N.; Villegas, I. F.; Benedictus, R. Characterisation of crystallinity at the interface of ultrasonically welded carbon fibre PPS joints. *Composites, Part A* **2019**, *125*, No. 105574.

(48) Volkov, S. S. Analysis of the process of heat generation in ultrasonic welding of plastics. *Weld. Int.* **2015**, *29*, 321−324.

(49) Kim, Y. H.; Wool, R. P. A theory of healing at a polymer-polymer interface. *Macromolecules* **1983**, *16*, 1115−1120.

(50) Ageorges, C.; Ye, L.; Hou, M. Advances in fusion bonding techniques for joining thermoplastic matrix composites: a review. *Composites, Part A* **2001**, *32*, 839−857.

(51) Meenakshisundaram, V.; Hung, J. H.; Patra, T. K.; Simmons, D. S. Designing Sequence-Specific Copolymer Compatibilizers Using a Molecular-Dynamics-Simulation-Based Genetic Algorithm. *Macromolecules* **2017**, *50*, 1155−1166.